

PAPER • OPEN ACCESS

# Detecting ultrathin ice on materials for optical coatings at cryogenic temperatures

To cite this article: Michele Magnozzi *et al* 2023 *J. Phys. D: Appl. Phys.* **56** 475105

View the [article online](#) for updates and enhancements.

## You may also like

- [Effect of Amphotericin B antibiotic on the properties of model lipid membrane](#)  
S Kiryakova, M Dencheva-Zarkova and J Genova
- [Corrigendum: A new approach for improving global critical current density in  \$\text{Fe}\(\text{Se}\_{0.5}\text{Te}\_{0.5}\)\$  polycrystalline materials](#)  
A Palenzona, A Sala, C Bernini et al.
- [Evidence of a miscibility gap in the  \$\text{FeTe}\_{1-x}\text{Se}\_x\$  polycrystalline samples prepared with a melting process](#)  
A Sala, A Palenzona, C Bernini et al.



## 244th ECS Meeting

Gothenburg, Sweden • Oct 8 – 12, 2023

Early registration pricing ends  
September 11

Register and join us in advancing science!



[Learn More & Register Now!](#)

# Detecting ultrathin ice on materials for optical coatings at cryogenic temperatures

Michele Magnozzi<sup>1,2,\*</sup> , Francesco Bisio<sup>3</sup> , Gianluca Gemme<sup>2</sup> , Massimo Granata<sup>4</sup> ,  
Christophe Michel<sup>4</sup> , Laurent Pinard<sup>4</sup>  and Maurizio Canepa<sup>1,\*</sup> 

<sup>1</sup> OptMatLab, Dipartimento di Fisica, Università di Genova, via Dodecaneso 33, 16146 Genova, Italy

<sup>2</sup> Istituto Nazionale di Fisica Nucleare, Sezione di Genova, via Dodecaneso 33, 16146 Genova, Italy

<sup>3</sup> CNR-SPIN, C.so Perrone 24, 16152 Genova, Italy

<sup>4</sup> Laboratoire des Matériaux Avancés - IP2I, CNRS, Université de Lyon, Université Claude Bernard Lyon 1, F-69622 Villeurbanne, France

E-mail: [magnozzi@fisica.unige.it](mailto:magnozzi@fisica.unige.it) and [canepa@fisica.unige.it](mailto:canepa@fisica.unige.it)

Received 28 April 2023, revised 24 July 2023

Accepted for publication 11 August 2023

Published 29 August 2023



## Abstract

The performance of optical cavities in gravitational wave detectors (GWD) is negatively affected by the growth of ice layers when operating at cryo temperatures. Loss of performance begins when the ice overlayer is only a few-nm thick. Careful planning is then required to minimize, monitor and take into account the presence of ultrathin ice on cryo-cooled optical surfaces. Here we employed spectroscopic ellipsometry (SE) to study icing on the surfaces of SiO<sub>2</sub> and Ti:Ta<sub>2</sub>O<sub>5</sub> thin films, two materials used in the high-reflective mirrors of current GWD. SE measurements were performed at 75 K. The data presented suggest that SE is a most convenient tool to monitor *in operando* the ice formation on the surfaces of GWD mirrors. Furthermore, ultrathin ice layers can affect the evaluation of the optical properties of materials at low temperatures, a valuable task for those next-generation GWD that will operate at cryogenic temperatures. The characterization of an ultrathin ice overlayer (<10 nm) allowed to determine for the first time the low-temperature optical properties of Ti:Ta<sub>2</sub>O<sub>5</sub>. The same approach could be applied to determine the low-temperature optical properties of other dielectric films, thus helping to screen new materials for cryo-operated GWD mirrors.

**Keywords:** ultrathin ice, icing, spectroscopic ellipsometry, optical coatings, cryogenic temperatures, gravitational wave detectors, Einstein Telescope

(Some figures may appear in colour only in the online journal)

## 1. Introduction

The KAGRA gravitational-wave detector (GWD) is currently operating at cryogenic temperature [1] and possible future

detectors, such as the low-frequency interferometer of Einstein Telescope [2, 3] and LIGO Voyager [4], will also operate at cryogenic temperature according to their current design. The low temperature of the mirrors, even in ultra-high vacuum environment, can induce the physisorption of molecular species leading to the growth of a cryodeposit layer over time. This overlayer, which is predominantly composed of water ice, adds an undesired contribution to the optical absorption of the coatings forming the mirrors, and affects their reflectivity. For instance KAGRA, the most recently-built GWD, has been reported to suffer from a loss of performance due to

\* Authors to whom any correspondence should be addressed.



Original Content from this work may be used under the terms of the [Creative Commons Attribution 4.0 licence](https://creativecommons.org/licenses/by/4.0/). Any further distribution of this work must maintain attribution to the author(s) and the title of the work, journal citation and DOI.

the progressive growth of an ice layer on the surface of its main mirrors [5–7]. Given the characteristics of GWD, such as the very large volume of the chambers that host the main mirrors, it is unlikely that the issue of icing can be completely avoided [8], at least with passive methods. Therefore, it becomes necessary to characterize, monitor and control the ice layer even when its thickness is very small, as it has been demonstrated that even a few nm thick ice layer causes large optical losses in GWD applications [7, 9].

The control of icing is also important to correctly design the mirrors operating at cryo temperatures. Design relies—among other things—on the low-temperature optical properties of the materials composing the mirrors, that are to be obtained through dedicated characterizations; however, these can be altered by the presence of ice overlayers, especially when the materials under investigation are in the form of thin films.

Spectroscopic ellipsometry (SE) is a well-proven technique to determine the optical properties and thickness of thin and ultrathin films [10–13], allowing the determination of the thickness with a resolution well below 1 nm in single-layer as well as multi-layer structures [14–16]. Moreover, SE can be implemented in cryogenic setups, so that SE data can be acquired while keeping the sample at cryogenic temperatures [9, 17], and therefore is an ideal tool to characterize and monitor thin and ultrathin ice layers.

In this work, we have characterised with SE the ultrathin ice layers on surfaces cooled down to liquid nitrogen temperature. We studied thin films of SiO<sub>2</sub> and Ti:Ta<sub>2</sub>O<sub>5</sub>, that is, the two materials that currently constitute the high-reflective mirrors in GWD. In particular, Ti:Ta<sub>2</sub>O<sub>5</sub> is subject to intense research with the aim to better understand and improve its optical properties for the purposes of the GWD [18–21]. To the knowledge of the authors, we report for the first time the optical properties of titania-doped tantala at cryogenic temperature in the near-infrared spectral range. The approach presented in this paper could be used to determine the low-temperature optical properties of other materials, that have been proposed for future cryo-operated GWD mirrors [22–24].

## 2. Methods

### 2.1. Materials

The silicon sample for the study of icing was manufactured by Siltronic and had the following characteristics: P-doped, resistivity  $\rho$ :  $<1 \Omega \cdot \text{cm}$ , orientation: (100)+/−0.5°, thickness: 0.5 mm. The titania-doped tantala film was deposited at the Laboratoire des Matériaux Avancés (<http://lma.in2p3.fr/>) on the silicon sample described above, by means of ion beam sputtering (IBS). IBS was performed inside the so-called Grand Coater, a custom-made coater machine where the actual mirrors for GWD are produced [25]. All samples studied in this work have size of  $1 \times 1 \text{ cm}^2$ .

### 2.2. Experimental methods

The SE data were acquired by means of a J.A. Woollam Variable Angle Spectroscopic Ellipsometer (VASE). The

present experiment focuses on the spectral range 1100–2450 nm, which is suitable for the GWD application as the operating wavelength for next generation GWD may change from the current 1064 nm, with 1550 and 2000 nm as likely options [3]. Acquired SE spectra contain 1 datapoint per nm, while the spectral bandwidth of the VASE is approximately 2 nm. The samples were cooled in an Oxford CF-V cryostat equipped with optical windows for SE measurements. The angle of incidence for the SE measurements was 45°. A scheme of the experimental setup composed of VASE and cryostat is shown in figure 1, left. An ellipsometry measurement yields  $\Delta$  and  $\Psi$ , the so-called ellipsometric angles that are defined according to the equation:

$$\tan \Psi e^{i\Delta} = \frac{|r_p|}{|r_s|} e^{i(\delta_p - \delta_s)} \quad (1)$$

where  $r_s$  ( $r_p$ ) is the  $s$ - ( $p$ )-polarized complex Fresnel reflection coefficient of the system.

Spectroscopic data are analyzed by fitting an optical model to experimental data. The quality of data fitting is estimated through minimization of the mean squared error (MSE), defined as:

$$\begin{aligned} \text{MSE} &= \sqrt{\frac{1}{2N - M} \cdot \sum_{i=1}^N \left[ \left( \frac{\Psi_i^{\text{exp}} - \Psi_i^{\text{calc}}}{\sigma_{\Psi,i}^{\text{exp}}} \right)^2 + \left( \frac{\Delta_i^{\text{exp}} - \Delta_i^{\text{calc}}}{\sigma_{\Delta,i}^{\text{exp}}} \right)^2 \right]} \end{aligned} \quad (2)$$

where  $\sigma_{\Psi,i}^{\text{exp}}$  and  $\sigma_{\Delta,i}^{\text{exp}}$  are the standard deviations of the experimental  $\Psi_i$  and  $\Delta_i$ ,  $N$  is the number of ( $\Psi$ ,  $\Delta$ ) pairs, and  $M$  is the number of fitted parameters in the model.

SE has already been successfully exploited to determine the optical properties of titania [26–30] and tantala [31–35] at room temperature; it constitutes a valid tool to investigate those properties also at cryogenic temperatures.

Samples were pre-treated with a mild annealing at 373 K overnight to reduce ambient molecular contamination [17], then cooled to 75 K. Pressure inside the cryostat was  $1.3 \times 10^{-5}$  mbar at the beginning of cooling and became lower than  $2.5 \times 10^{-6}$  mbar at 75 K.  $\Delta$ ,  $\Psi$  and temperature were continuously monitored during the cooling, as exemplified in figure 1(right). The pressure inside the cryostat is higher than that used in KAGRA, the latter being in the order of  $10^{-8}$  mbar. Here, we intend to present SE as a convenient tool to monitor *in operando* the formation of ultrathin ice layers. The implications of this work remain valid in the case of lower pressure, which would cause a lower ice growth rate.

The investigation of icing and optical properties of materials at low temperatures requires two reference datasets at room temperature, namely, one on the sample in air, and another on the sample inside the cryostat. This ensures the identification of any temperature-induced variations in the low-temperature dataset and also allows one to identify and correct any spurious effect due to operation of the cryostat, as for example the windows effects [13].

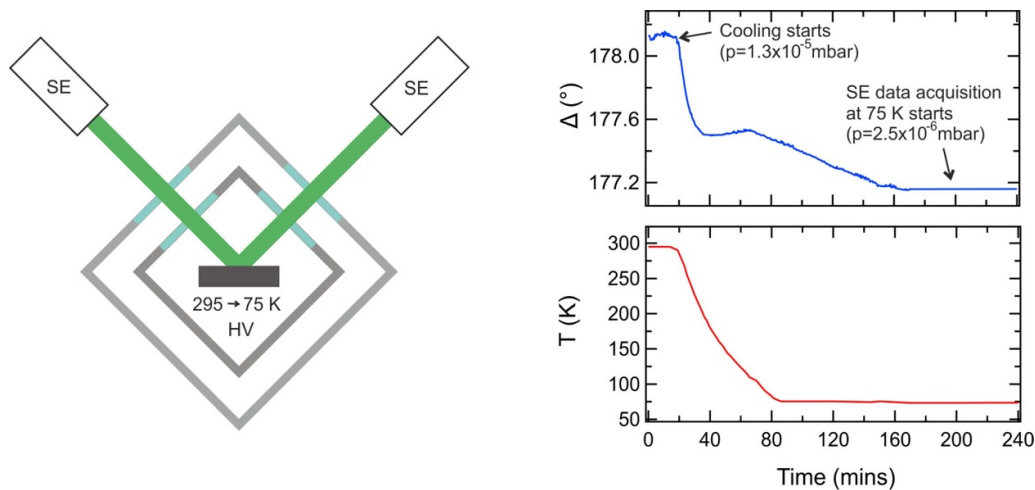


**Figure 1.** Left: Simplified scheme of the experimental setup showing the optical cryostat and the geometry for SE measurements. Right: example of real-time monitoring of  $\Delta$  at 1000 nm (upper graph) and temperature (lower graph) when cooling samples down to 75 K. The decrease in  $\Delta$  starts from the very early stages of cooling.

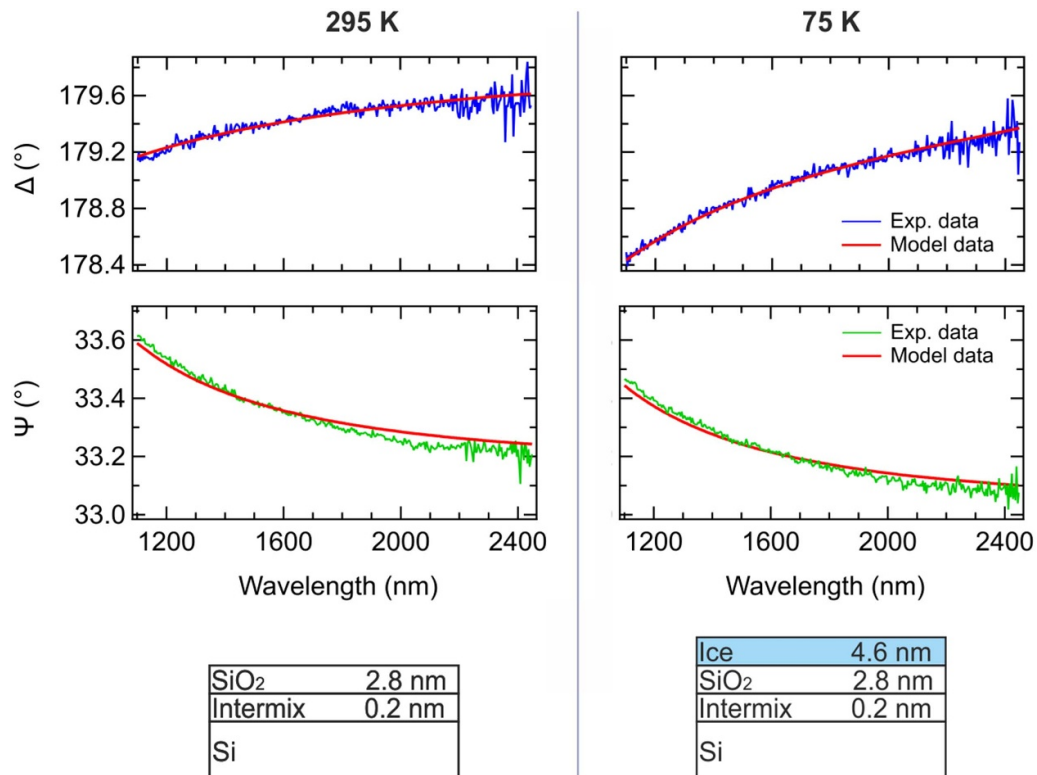


**Figure 2.** SE experimental and model data on Si at RT (left column) and at 75 K (right column). The bottom row in the figure represents the structure of the model used to calculate the SE data reported in the graphs above.

### 3. Results and discussion

We first investigated icing on a silicon wafer with native silicon oxide, a task which requires SE data both at room temperature and at 75 K. Modeling the SE data at room temperature [36] yielded excellent results, as shown in figure 2 (left). The sample was then cooled and SE data were acquired at 75 K (figure 2, right).  $\Delta$  decreased by about  $0.8^\circ$  at 1100 nm when going from RT to 75 K, a sizable variation which can be

interpreted through proper data modelling. The optical properties of Si at 75 K, as reported by Frey *et al* [37], were fed into the optical model. On the other hand, the optical response of the ultrathin native SiO<sub>2</sub> layer was assumed to be temperature-independent [38]. The model built by using the above-mentioned data was not able to reproduce the experimental low-T SE data, as shown in figure 3, right (dashed curve). Given the experimental conditions (low temperature, high vacuum environment) we attribute the mismatch to icing,

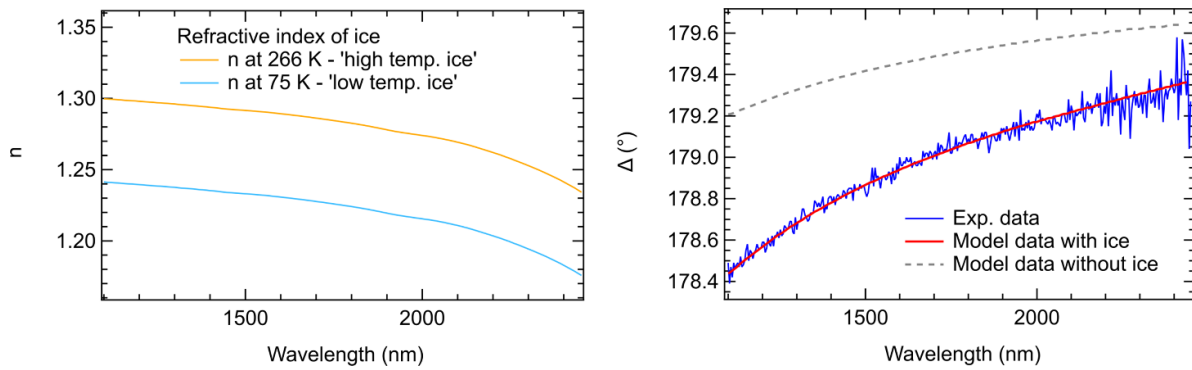


**Figure 3.** Left: refractive index of ice at 266 K (orange line) and at 75 K (light blue line). Right: Experimental  $\Delta$  at 75 K (blue line); calculated  $\Delta$  including the ice layer (red line); calculated  $\Delta$  without the ice layer (gray dotted line).

and therefore upgrade the model to take into account an ultrathin ice overlayer. We note that  $\Delta$ , much more than  $\Psi$ , is sensitive to small thickness variations when investigating thin transparent films, therefore, we look mainly at the variations in  $\Delta$  to quantify the presence of ice.

The optical properties of ice have been studied in a number of different experimental conditions, including pressure, temperature, and spectral range [39–42]. The refractive index was found not to vary with the ice phase [42]; it decreases—along with the density—with temperature [41]. In other words, ice formed at higher temperatures has a higher density and a higher refractive index with respect to ice formed at lower temperatures. In our experiments, the  $\Delta$  variations associated to the ice growth occur already during the cooling process, i.e. when the temperature decreases, as clearly shown in figure 1(right), meaning that no single temperature can be associated to the ice formation in this case. In order to estimate the refractive index of the ice in our experiments, we conveniently identify two types of ice, namely, the ‘high-temperature’ ice and ‘low-temperature’ ice, that will be described below. Then, we can safely assume that the refractive index of the ice in our experiment lies between that of the ‘high-temperature’ ice and ‘low-temperature’ ice.

According to Warren [39, 43], the refractive index of ice at 266 K monotonously decreases in the spectral range of interest (1100–2450 nm), and the extinction coefficient remains below  $<3 \times 10^{-3}$ . In these conditions, the Cauchy dispersion model is appropriate to describe the optical response of the material. We use Warren’s data as a reference for the ‘high-temperature’ ice. Kofman *et al* [41] determined the refractive index of ice at 632.8 nm at temperatures down to 10 K; at that wavelength, their data indicate that refractive index of ice at 75 K is reduced by about 0.058 with respect to Warren’s data. The refractive index of ice is featureless and only slightly dispersing from 632 to 2500 nm, therefore we can tentatively derive the refractive index of ‘low-temperature’ ice by subtracting 0.058 from Warren’s data. The refractive indices corresponding to the ‘high-’ and ‘low-temperature’ ice are reported in figure 3, left.

Having fixed two boundaries for the refractive index of ice in our experiment, we can now build the optical model and fit the thickness of the ice overlayer. When considering the

overlayer as entirely composed of ‘low-temperature’ ice, we obtain a thickness of  $4.6 \pm 0.2$  nm. Conversely, if we consider the overlayer as purely ‘high-temperature’ ice, we obtain  $4.0 \pm 0.2$  nm. The agreement with the experimental data was equivalent in the two cases (MSE = 0.42). We can therefore conclude that the thickness of the ice overlayer in this experiment lies between 3.8 and 4.8 nm. By relating such thickness to the corresponding variation induced in  $\Delta$ , we can estimate that the lowest detection limit of ice by means of SE in these experimental conditions is well below 1 nm. We note that ice detected by SE in this work is sufficiently thick to be considered as a material with clearly-defined, isotropic dielectric properties, i.e. not the atomic clusters or sub-monolayer entities that can occur in the very early stages of icing on a clean surface [44–47]. Similarly, we did not consider any possible chemical interface between the substrate and the overlayer [48, 49].

The method used to study icing on a well-known system (silicon/silicon oxide) can be generalized to investigate the low-temperature optical properties of other materials. Here, we consider the case of titania-doped tantala, a material which is a key component of the mirrors for GWDs. The broadband optical properties of this sample in ambient atmosphere and at room temperature were carefully determined in a previous work [21, 50]. However, unlike the case of silicon, the broadband optical properties of titania-tantala at low temperatures have not been reported yet. Previous data on pure tantala, obtained within a very limited temperature range, suggest that the temperature-induced variation in the refractive index of that material are small [51]; as a consequence, the need to distinguish those variations from spurious effects at low temperatures (i.e. the growth of an ice overlayer) is evident. We build on the knowledge previously validated on silicon to determine both the optical constants of titania-tantala at 75 K, and the thickness of the ice overlayer that forms on top of it. The titania-tantala film was grown on a silicon substrate which is identical to the one considered in the first part of this work. The SE measurements inside the cryostat, both at room temperature and at 75 K, followed the same procedures described earlier for the silicon sample. An optical model was built where the two unknown parameters were the thickness of the ultrathin ice layer and the refractive index of the titania-tantala;

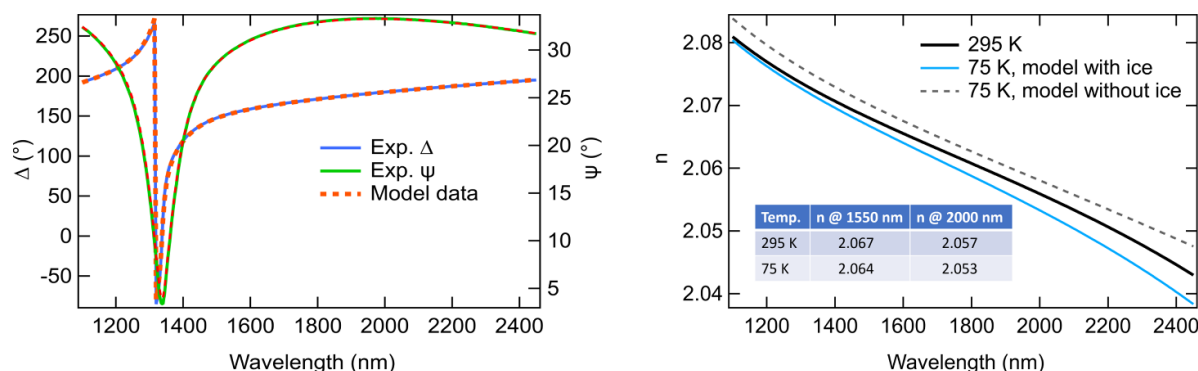


**Figure 4.** Left: experimental (continuous lines) and best-fit model (red dotted lines) SE data of annealed titania:tantala coating at 75 K. Right: refractive index of titania:tantala calculated at room temperature (black line), at 75 K without considering the ultrathin ice layer (grey dotted curve), and at 75 K considering the ultrathin ice layer (blue curve). The table inset reports the refractive index of titania:tantala at 1550 and 2000 nm, obtained from the model with ice. At 75 K, the measured thickness of the ice layer was  $8.5 \pm 0.8$  nm.

concerning the refractive index of ice, the ‘high-temperature’ and ‘low-temperature’ cases were replicated to estimate the uncertainty on the results.

The model agreement with the experimental data was good ( $MSE = 1.7$ ), as reported in figure 4(left). The measured thickness of ice layer was  $8.5 \pm 0.8$  nm. The refractive index of the titania:tantala decreased slightly when going from RT to 75 K, as reported in figure 4(right). On the other hand, if the presence of ice is not taken into account, the resulting refractive index at 75 K (gray dotted line in figure 4, right) turns out to be higher than that at room temperature, that is, the sign of the variations in refractive index changes when ice is not considered. The model without ice resulted in  $MSE = 3.4$ , that is, twice as large as that obtained from the model with ice. Therefore, the most accurate determination of refractive index at low temperature is achieved by taking into account the presence of an ice overlayer. The information on the refractive index of titania–tantala determined in this work can be combined with the mechanical loss measured at cryogenic temperatures [52–55], to provide a comprehensive description of the materials’ properties for mirrors in cryogenic GWD [56].

#### 4. Concluding remarks

The first cryo-operated GWD has shown that the formation of cryodeposits on the surface of cooled mirrors has detrimental effects on the performance of GWD [5]. More generally, ultrathin ice layers also hinder the evaluation of optical properties of materials at cryo temperatures. Therefore, in both cases, it is necessary to detect and monitor the thickness of the ultrathin ice layers. In this work, we proved that ultrathin ( $<10$  nm) ice layers can easily and unambiguously be identified on surfaces of thin films of oxides by means of SE. Samples were kept at low temperatures by means of a suitable cryostat. By quantifying the presence of ice, the accuracy in determining the temperature-dependent optical properties of materials for GWD mirrors is improved. In this way we obtained the first characterization of the low-temperature optical properties of titania-doped tantala, a strategic material for GWD. We note that the same approach can

be applied to any dielectric thin film indicated as a potential candidate for the high-index constituent of mirror coatings [24]. The results of this work suggest that SE—or even single-wavelength ellipsometry—is most suitable to monitor *in operando* the growth of ice layers on the mirrors of future GWD working at low temperatures, such as the low-frequency detector of the Einstein Telescope according to its current design [3].

#### Data availability statement

The data that support the findings of this study are available upon reasonable request from the authors.

#### Acknowledgments

We gratefully acknowledge the Fondazione San Paolo (Progetto MIDA) and the Project Einstein Telescope Infrastructure Consortium (ETIC) (IR0000004) - MUR call n. 3264 PNRR, Miss. 4 - Comp. 2, Line 3.1. We acknowledge the support of the Italian Ministry for University and Research (MIUR) through the Project ‘Dipartimenti di Eccellenza 2017–2022’ (DIFILAB). We thank the Virgo Coating R&D collaboration for helpful discussions and Ennio Vigo for technical support.

#### Conflicts of interest

There are no conflicts of interest to declare.

#### ORCID iDs

Michele Magnozzi <https://orcid.org/0000-0003-4512-8430>

Francesco Bisio <https://orcid.org/0000-0003-1776-3023>

Gianluca Gemme <https://orcid.org/0000-0002-1127-7406>

Massimo Granata <https://orcid.org/0000-0003-3275-1186>

Christophe Michel <https://orcid.org/0000-0003-0606-725X>

Laurent Pinard  <https://orcid.org/0000-0002-8842-1867>  
 Maurizio Canepa  <https://orcid.org/0000-0002-5148-1233>

## References

- [1] Akutsu T *et al* 2019 KAGRA: 2.5 generation interferometric gravitational wave detector *Nat. Astron.* **3** 35–40
- [2] Maggiore M *et al* 2020 Science case for the Einstein telescope *J. Cosmol. Astropart. Phys.* **2020** 050
- [3] ET Editorial Team 2020 Design report update 2020 for the Einstein Telescope *ET public document, Technical Documentation System* Number: ET-0007B-20
- [4] Adhikari R X *et al* 2020 A cryogenic silicon interferometer for gravitational-wave detection *Class. Quantum Grav.* **37** 165003
- [5] Hasegawa K, Akutsu T, Kimura N, Saito Y, Suzuki T, Tomaru T, Ueda A and Miyoki S 2019 Molecular adsorbed layer formation on cooled mirrors and its impacts on cryogenic gravitational wave telescopes *Phys. Rev. D* **99** 022003
- [6] Steinlechner J and Martin I W 2019 Thermal noise from icy mirrors in gravitational wave detectors *Phys. Rev. Res.* **1** 013008
- [7] Tanioka S, Hasegawa K and Aso Y 2020 Optical loss study of molecular layer for a cryogenic interferometric gravitational-wave detector *Phys. Rev. D* **102** 022009
- [8] Grado A *et al* 2023 Ultra high vacuum beam pipe of the Einstein Telescope project: challenges and perspectives *J. Vac. Sci. Technol. B* **41** 024201
- [9] Tanioka S and Aso Y 2021 Optical loss study of the cryogenic molecular layer using a folded cavity for future gravitational-wave detectors *Opt. Express* **29** 6780–93
- [10] Fujiwara H 2007 *Spectroscopic Ellipsometry* (Wiley)
- [11] Tompkins H G and Hilfiker J N 2016 *Spectroscopic Ellipsometry. Practical Application to Thin Film Characterization* (Momentum Press Engineering)
- [12] Canepa M 2013 *Surface Science Techniques* ed G Bracco and B Holst (Springer) pp 99–135
- [13] Magnozzi M, Haghighian N, Miseikis V, Cavalleri O, Coletti C, Bisio F and Canepa M 2017 Fast detection of water nanopockets underneath wet-transferred graphene *Carbon* **118** 208–14
- [14] Losurdo M *et al* 2009 Spectroscopic ellipsometry and polarimetry for materials and systems analysis at the nanometer scale: state-of-the-art, potential and perspectives *J. Nanopart. Res.* **11** 1521–54
- [15] Magnozzi M *et al* 2018 Optical properties of amorphous SiO<sub>2</sub>-TiO<sub>2</sub> multi-nanolayered coatings for 1064 nm mirror technology *Opt. Mater.* **75** 94–101
- [16] Magnozzi M, Ferrera M, Piccinini G, Pace S, Forti S, Fabbri F, Coletti C, Bisio F and Canepa M 2020 Optical dielectric function of two-dimensional WS<sub>2</sub> on epitaxial graphene *2D Mater.* **7** 025024
- [17] Zollner S, Abadizaman F, Emminger C and Samarasingha N 2022 Spectroscopic ellipsometry from 10 to 700 K *Adv. Opt. Technol.* **11** 117–35
- [18] Granata M *et al* 2020 Amorphous optical coatings of present gravitational-wave interferometers *Class. Quantum Grav.* **37** 095004
- [19] Fazio M A, Vajente G, Ananyeva A, Markosyan A, Bassiri R, Fejer M M and Menoni C S 2020 Structure and morphology of low mechanical loss TiO<sub>2</sub>-doped Ta<sub>2</sub>O<sub>5</sub> *Opt. Mater. Express* **10** 1687–703
- [20] Fazio M A, Vajente G, Yang L, Ananyeva A and Menoni C S 2022 Comprehensive study of amorphous metal oxide and Ta<sub>2</sub>O<sub>5</sub>-based mixed oxide coatings for gravitational-wave detectors *Phys. Rev. D* **105** 102008
- [21] Amato A, Magnozzi M, Shcheblanov N, Lemaitre A, Cagnoli G, Granata M, Michel C, Gemme G, Pinard L and Canepa M 2023 Enhancing titania-tantala amorphous materials as high-index layers in Bragg reflectors of gravitational-wave detectors *ACS Appl. Opt. Mater.* **1** 395–402
- [22] Kuo L-C, Pan H-W, Chang C-L and Chao S 2019 Low cryogenic mechanical loss composite silica thin film for low thermal noise dielectric mirror coatings *Opt. Lett.* **44** 247–50
- [23] Craig K *et al* 2019 Mirror coating solution for the cryogenic Einstein Telescope *Phys. Rev. Lett.* **122** 231102
- [24] Granata M *et al* 2020 Progress in the measurement and reduction of thermal noise in optical coatings for gravitational-wave detectors *Appl. Opt.* **59** A229–35
- [25] Collaboration T V *et al* The VIRGO Collaboration 2004 *Class. Quantum Grav.* **21** S935
- [26] Bundesmann C, Eichentopf I-M, Mändl S and Neumann H 2008 Stress relaxation and optical characterization of TiO<sub>2</sub> and SiO<sub>2</sub> films grown by dual ion beam deposition *Thin Solid Films* **516** 8604–8
- [27] Jiang H-Q, Wei Q, Cao Q-X and Yao X 2008 Spectroscopic ellipsometry characterization of TiO<sub>2</sub> thin films prepared by the sol-gel method *Ceram. Int.* **34** 1039–42
- [28] Toccalfondi C, Uttiya S, Cavalleri O, Gemme G, Barborini E, Bisio F and Canepa M 2014 Optical properties of nanogranular and highly porous TiO<sub>2</sub> thin films *J. Phys. D: Appl. Phys.* **47** 485301
- [29] Bundesmann C, Lautenschläger T, Spemann D, Finzel A, Thelander E, Mensing M and Frost F 2017 Systematic investigation of the properties of TiO<sub>2</sub> films grown by reactive ion beam sputter deposition *Appl. Surf. Sci.* **421** 331
- [30] Jaiswal J, Mourya S, Malik G and Chandra R 2019 Ellipsometric investigation of room temperature grown highly-oriented anatase TiO<sub>2</sub> thin films *J. Electron. Mater.* **48** 1223–34
- [31] Franke E, Trimble C L, DeVries M J, Woollam J A, Schubert M and Frost F 2000 Dielectric function of amorphous tantalum oxide from the far infrared to the deep ultraviolet spectral region measured by spectroscopic ellipsometry *J. Appl. Phys.* **88** 5166–74
- [32] Stenzel O *et al* 2009 The correlation between mechanical stress, thermal shift and refractive index in HfO<sub>2</sub>, Nb<sub>2</sub>O<sub>5</sub>, Ta<sub>2</sub>O<sub>5</sub> and SiO<sub>2</sub> layers and its relation to the layer porosity *Thin Solid Films* **517** 6058–68
- [33] Prato M, Chincarini A, Gemme G and Canepa M 2011 Gravitational waves detector mirrors: spectroscopic ellipsometry study of Ta<sub>2</sub>O<sub>5</sub> films on SiO<sub>2</sub> substrates *Thin Solid Films* **519** 2877–80
- [34] Amato A *et al* 2019 Optical properties of high-quality oxide coating materials used in gravitational-wave advanced detectors *J. Phys. Mater.* **2** 035004
- [35] Chen X, Bai R and Huang M 2019 Optical properties of amorphous Ta<sub>2</sub>O<sub>5</sub> thin films deposited by RF magnetron sputtering *Opt. Mater.* **97** 109404
- [36] Herzinger C M, Johs B, McGahan W A, Woollam J A and Paulson W 1998 Ellipsometric determination of optical constants for silicon and thermally grown silicon dioxide via a multi-sample, multi-wavelength, multi-angle investigation *J. Appl. Phys.* **83** 3323–36
- [37] Frey B J, Leviton D B and Madison T J 2006 Temperature-dependent refractive index of silicon and germanium *Proc. SPIE* **6273** 62732J
- [38] Lautenschläger P, Garriga M, Vina L and Cardona M 1987 Temperature dependence of the dielectric function and interband critical points in silicon *Phys. Rev. B* **36** 4821–30
- [39] Warren S G 1984 Optical constants of ice from the ultraviolet to the microwave *Appl. Opt.* **23** 1206–25

- [40] Dohnálek Z, Kimmel G A, Ayotte P, Smith R S and Kay B D 2003 The deposition angle-dependent density of amorphous solid water films *J. Chem. Phys.* **118** 364–72
- [41] Kofman V, He J, ten Kate I L and Linnartz H 2019 The refractive index of amorphous and crystalline water ice in the UV-vis *Astrophys. J.* **875** 131
- [42] Stubbing J W, McCoustra M R S and Brown W A 2020 A new technique for determining the refractive index of ices at cryogenic temperatures *Phys. Chem. Chem. Phys.* **22** 25353–65
- [43] Warren S G 2019 Optical properties of ice and snow *Phil. Trans. R. Soc. A* **377** 20180161
- [44] Thiel P A and Madey T E 1987 The interaction of water with solid surfaces: fundamental aspects *Surf. Sci. Rep.* **7** 211–385
- [45] Henderson M A 2002 The interaction of water with solid surfaces: fundamental aspects revisited *Surf. Sci. Rep.* **46** 1–308
- [46] Mu R, Zhao Z-J, Dohnálek Z and Gong J 2017 Structural motifs of water on metal oxide surfaces *Chem. Soc. Rev.* **46** 1785–806
- [47] Shimizu T K, Maier S, Verdager A, Velasco-Velez J-J and Salmeron M 2018 Water at surfaces and interfaces: from molecules to ice and bulk liquid *Prog. Surf. Sci.* **93** 87–107
- [48] Canepa M, Cantini P, Narducci E, Salvietti M, Terreni S and Mattera L 1995 Coexistence of OH phases on Ag(110) *Surf. Sci.* **343** 176–84
- [49] Canepa M, Mattera L and Narducci E 1997 Recombination of hydroxyl phases on Ag(110): coexistence of long-range ordered domains of atomic oxygen and hydroxyl *Surf. Sci.* **371** 431–7
- [50] Magnozzi M, Amato A, Shcheblanov N, Lemaitre A, Cagnoli G, Granata M, Michel C, Gemme G, Pinard L, Canepa M 2022 Effects of mixing and annealing on the optical properties of TiO<sub>2</sub>:Ta<sub>2</sub>O<sub>5</sub> amorphous oxide coatings *Optical Interference Coatings Conf. (OIC) 2022* p WB.7
- [51] Chu A K, Lin H C and Cheng W H 1997 Temperature dependence of refractive index of Ta<sub>2</sub>O<sub>5</sub> dielectric films *J. Electron. Mater.* **26** 889–92
- [52] Martin I *et al* 2008 Measurements of a low-temperature mechanical dissipation peak in a single layer of Ta<sub>2</sub>O<sub>5</sub> doped with TiO<sub>2</sub> *Class. Quantum Grav.* **25** 055005
- [53] Granata M *et al* 2013 Cryogenic measurements of mechanical loss of high-reflectivity coating and estimation of thermal noise *Opt. Lett.* **38** 5268–71
- [54] Hirose E *et al* 2014 Mechanical loss of a multilayer tantala/silica coating on a sapphire disk at cryogenic temperatures: toward the KAGRA gravitational wave detector *Phys. Rev. D* **90** 102004
- [55] Robinson J M *et al* 2021 Thermal noise and mechanical loss of SiO<sub>2</sub>/Ta<sub>2</sub>O<sub>5</sub> optical coatings at cryogenic temperatures *Opt. Lett.* **46** 592–5
- [56] Hirose E, Billingsley G, Zhang L, Yamamoto H, Pinard L, Michel C, Forest D, Reichman B and Gross M 2020 Characterization of core optics in gravitational-wave detectors: case study of KAGRA sapphire mirrors *Phys. Rev. Appl.* **14** 014021